



Particulate emissions  
from Athabasca oil  
sands

S. G. Howell et al.

# An airborne assessment of atmospheric particulate emissions from the processing of Athabasca oil sands

S. G. Howell<sup>1</sup>, A. D. Clarke<sup>1,2</sup>, S. Freitag<sup>2</sup>, C. S. McNaughton<sup>1,\*</sup>, V. Kapustin<sup>1</sup>,  
V. Brekovskikh<sup>1</sup>, J.-L. Jimenez<sup>3</sup>, and M. J. Cubison<sup>3,\*\*</sup>

<sup>1</sup>University of Hawaii Department of Oceanography, USA

<sup>2</sup>University of Hawaii Department of Meteorology, USA

<sup>3</sup>Cooperative Institute for Research in the Environmental Sciences and Department of Chemistry and Biochemistry, University of Colorado, Boulder, Colorado, USA

\* now at: Golder Associates Ltd., Saskatoon, Saskatchewan, Canada

\*\* now at: Tofwerk AG, Thun, Switzerland

Received: 31 July 2013 – Accepted: 1 August 2013 – Published: 15 August 2013

Correspondence to: S. G. Howell (sghowell@hawaii.edu)

Published by Copernicus Publications on behalf of the European Geosciences Union.

Title Page

Abstract

Introduction

Conclusions

References

Tables

Figures



Back

Close

Full Screen / Esc

Printer-friendly Version

Interactive Discussion



## Abstract

During the Arctic Research of the Composition of the Troposphere from Aircraft and Satellites (ARCTAS) campaign, two NASA research aircraft, a DC-8 and a P-3B, were outfitted with extensive trace gas (the DC-8) and aerosol (both aircraft) instrumentation. Each aircraft spent about a half hour sampling air around the oil sands mining and upgrading facilities near Ft. McMurray, Alberta, Canada. The DC-8 circled the area, while the P-3B flew directly over the upgrading plants, sampling close to the exhaust stacks, then headed downwind to monitor the aerosol as it aged. At short range, the plume from the oil sands is a complex mosaic of freshly nucleated ultrafine particles from a  $\text{SO}_2$  and  $\text{NO}_2$ -rich plume, fly ash and soot from industrial processes, and dust from dirt roads and mining operations. Shortly downwind, organic aerosol appears in quantities that rival  $\text{SO}_4^-$ , either as volatile organic vapors condense or as they react with the  $\text{H}_2\text{SO}_4$ . The DC-8 pattern allowed us to integrate total flux from the oil sands facilities within about a factor of two uncertainty that spanned values consistent with 2008 estimates from reported  $\text{SO}_2$  and  $\text{NO}_2$  emissions. In contrast, CO fluxes exceeded reported regional emissions, due either to variability in production or sources missing from the emissions inventory. The conversion rate of  $\text{SO}_2$  to aerosol  $\text{SO}_4^-$  of  $\sim 6\%$  per hour is consistent with earlier reports, though OH concentrations are insufficient to accomplish this. Other oxidation pathways must be active. Altogether, organic aerosol and black carbon emissions from the oil sands operations are small compared with the forest fires present in the region during the summer. The oil sands do contribute significant sulfate and exceed fire production of  $\text{SO}_2$  by an order of magnitude.

## 1 Introduction

Canada's oil sand deposits represent 30% of total world oil reserves (Alboudwarej et al., 2006) and are estimated at about 180 billion barrels. Most of these resources are in Alberta near the Athabasca River. However, the bitumen contained within the

ACPD

13, 21301–21343, 2013

## Particulate emissions from Athabasca oil sands

S. G. Howell et al.

Title Page

Abstract

Introduction

Conclusions

References

Tables

Figures

◀

▶

◀

▶

Back

Close

Full Screen / Esc

Printer-friendly Version

Interactive Discussion



**Particulate emissions  
from Athabasca oil  
sands**

S. G. Howell et al.

Title Page

Abstract

Introduction

Conclusions

References

Tables

Figures

◀

▶

◀

▶

Back

Close

Full Screen / Esc

Printer-friendly Version

Interactive Discussion



sand is extremely viscous, requiring heat or solvents to extract from the sand. The surface mining operators (e.g., Syncrude Canada, Suncor Energy, Albian Sands Energy) extract the bitumen using a hot water process. About 80 % of the deposits are not recoverable by surface mining and require in-situ recovery using steam injection. Before the bitumen can be sent through pipelines and refined, it must be upgraded, a combination of processes that consume natural gas and produce synthetic crude oil and CO<sub>2</sub>.

There are many sources of aerosols and aerosol precursors in the oil sand extraction and upgrading processes. The bitumen itself releases SO<sub>2</sub>, H<sub>2</sub>S and light hydrocarbons as well as CO<sub>2</sub> and CO on heating (Strausz et al., 1977). Surface mining releases dust directly and road dust and soot are produced by trucks. Since the Athabasca bitumen contains approximately 5 % sulfur and 0.5 % nitrogen, the upgrading process can release large quantities of these as SO<sub>2</sub> and NO<sub>2</sub> as well as soot. The SO<sub>2</sub> forms sulphate aerosol at up to 6 % h<sup>-1</sup> (Cheng et al., 1987). Fly ash has been documented from a coke-burning power plant associated with the upgraders (Barrie, 1980).

Development of the oil sands began with the Great Canadian Oil Sands Company in 1967 but started expanding rapidly around 2000. As production has increased, the industry has invested heavily in emissions abatement equipment on existing facilities and state-of-the-art low emission technologies on new facilities in order to ensure regional air quality stays within regulated limits. Oil sands operators are also required to report emissions to the Environment Canada's National Pollutant Release Inventory (<http://www.ec.gc.ca/inrp-npri/>) and fund air quality monitoring in the region. As part of their response to environmental issues, the oil sands operators have provided capital and ongoing support for the Wood Buffalo Environmental Association (WBEA; <http://www.wbea.org/>) which is a collaboration of communities, environmental groups, industry, government and Aboriginal stakeholders. WBEA operates an environmental monitoring program that measures the ambient air quality at about 15 stations throughout the area and continuously monitors environmental effects of air emissions through the Terrestrial Environmental Effects Monitoring Program, which addresses

issues such as soil acidification, trace metals in foods harvested by Aboriginal communities, and vegetation stress. Data from many of these sites can be accessed directly through the WBEA website.

One of the unusual features of the oil sands facilities is their location in an area lacking large populations and other industrial facilities. This makes the emissions more obvious against a relatively clean background. Hence, the oil sands emissions can be discerned in global satellite maps of NO<sub>2</sub> and SO<sub>2</sub> (McLinden et al., 2012) even though total emissions are smaller than many urban regions. This input of pollutants into a nearly pristine area has been of concern since development began in the area. Studies of aerosol formation (Cheng et al., 1987), deposition (Barrie, 1980; Proemse et al., 2012b) and composition (Proemse et al., 2012a) have been ongoing as have air quality modeling efforts (Davies, 2012).

Despite this emphasis on measuring oil sands emissions, there had been no recent evaluations of them using an extensive airborne instrumentation suite until the summer of 2008, when the NASA DC-8 and P-3B research aircraft were deployed at the Canadian Forces Base Cold Lake in Alberta, Canada. The main focus of the project was to study smoke plumes from the forest fires that occur every year in Northern Canada (Jacob et al., 2010), but the two planes detoured one day to measure aerosol and trace gas emissions from the facilities near Ft. McMurray.

The gas phase data revealed two different types of plumes (Simpson et al., 2010). One was a broad plume that consisted primarily of light hydrocarbons, presumed to be either from the bitumen or the solvents used to mobilize it. The other was a more typically industrial plume with high concentrations of NO<sub>2</sub> and SO<sub>2</sub> together with CO, CO<sub>2</sub>, and a variety of alkanes, solvents, and halocarbons. The work reported here extends that analysis to include aerosol emissions.

**Particulate emissions from Athabasca oil sands**

S. G. Howell et al.

Title Page

Abstract

Introduction

Conclusions

References

Tables

Figures



Back

Close

Full Screen / Esc

Printer-friendly Version

Interactive Discussion



## 2 Experimental

The flights around the Ft. McMurray oil sands upgrading facilities took place on 10 July 2008. The DC-8 and P-3B took the opportunity to do a joint flight over the oil sands to perform an instrument intercomparison and a brief evaluation of the aerosol and gas emissions from the facilities there (Fig. 1). The DC-8 flew a loop around the facilities at about 350 m a.g.l., passing through the entire plume and providing upwind samples for contrast. The P-3B flew a figure 8, passing through visible plumes from the tallest stacks in the facilities (Fig. 2). The Syncrude plume was sampled twice at about 240 m a.g.l. and once at 625 m while the Suncor plume was sample once, at about 250 m. After the third Syncrude plume penetration, the P-3B turned downwind and followed the evolving plume.

In addition to the 10 July flights, there were 3 plume penetrations on other ARCTAS flights (Fig. 3). The P3-B descended into the mixed layer during transits from fire plume studies on 28 and 29 June, while the DC-8 flew a low pass early on 28 June looking for a fire plume from the previous day and coincidentally met the oil sands plume.

### 2.1 Instrumentation

The two aircraft had complementary payloads. The DC-8 was outfitted with an extensive suite of gas-phase and aerosol instruments. The P-3B had similar aerosol measurements and several radiation propagation measurements, but no gas phase capability beyond CO and O<sub>3</sub>. Both aircraft used the aerosol inlet characterized by McNaughton et al. (2007), who found that it efficiently conveyed dust particles of up to a few microns in diameter. Additional information and data from ARCTAS can be found at [http://www.espo.nasa.gov/arctas/airborne\_inst.php]. Rather than describing the entire set of measurements, a short description of the most relevant ones is included here.

Number concentrations measurements were almost identical on both aircraft. The concentration of particles > 3 nm were measured with TSI model 3025A Ultrafine Con-

## Particulate emissions from Athabasca oil sands

S. G. Howell et al.

Title Page

Abstract

Introduction

Conclusions

References

Tables

Figures



Back

Close

Full Screen / Esc

Printer-friendly Version

Interactive Discussion



**Particulate emissions  
from Athabasca oil  
sands**

S. G. Howell et al.

Title Page

Abstract

Introduction

Conclusions

References

Tables

Figures

◀

▶

◀

▶

Back

Close

Full Screen / Esc

Printer-friendly Version

Interactive Discussion

densation Nuclei (UCN) counters. Particles  $\gtrsim 10$  nm were measured with pair of TSI model 3010 Condensation Nuclei (CN) counters operated with a temperature difference of  $22^\circ\text{C}$  between saturator and condenser. One (called CNcold henceforth) had no additional heat applied to the inlet while the other had an inlet tube heated to  $350^\circ\text{C}$  for about 0.1 s to remove most volatile material (CNhot). CNhot is typically associated with combustion, as flames produce nonvolatile black carbon and organic material, though dust, seasalt, and volatile particles too large to evaporate entirely can also contribute (Clarke, 1991). Differences between UCN and CNcold show particles in the 3 to 10 nm range indicative of recent new particle formation (nucleation). UCN and CNcold suffered from saturation of the counters-concentrations so high that multiple particles were in the sensing volume simultaneously and were not counted properly. The counters used for CNcold and CNhot do not compensate for coincident particles, which becomes a problem at  $> 10 \times 10^3 \text{ cm}^{-3}$ . A correction algorithm was applied (Baron and Willeke, 2001), but the algorithm fails above about  $35 \times 10^3 \text{ cm}^{-3}$ , when particles are in the sampling volume  $\geq 50\%$  of the time. The UCN counter automatically compensates for coincident particles, but saturates at  $100 \times 10^3 \text{ cm}^{-3}$ .

Aerosol size distribution measurements differed modestly between the platforms. Both used Differential Mobility Analyzers (DMAs, TSI long DMA model 3081) for particles from  $\sim 10$  to 400 nm, Optical Particle Counters (OPCs) for rapid measurement of the the accumulation mode (0.2 to  $1 \mu\text{m}$ ), and Aerodynamic Particle Sizers (APS, TSI model 3321) to measure aerodynamic particle diameters between  $\sim 0.8 \mu\text{m} < D_{\text{ae}} < 10 \mu\text{m}$ . The DC-8 used a DMT UHSAS OPC, which resolves smaller particles (0.055 to  $1 \mu\text{m}$ ) at a higher rate (1 Hz) than the modified LAS-X OPC on the P3-B (0.2 to  $3 \mu\text{m}$ , 0.33 Hz), though the latter had a set of heated inlets that could explore volatility at 150, 300, and  $400^\circ\text{C}$  (residence times  $> 1$ ). The P-3B also had a TSI radial DMA with unheated and  $300^\circ\text{C}$ , 0.1 s inlets that spanned 10 to 200 nm.

Aerosol composition measurements were similar on the two aircraft. Non-refractory submicron composition was measured with Aerodyne High-Resolution Time-of-Flight Aerosol Mass Spectrometers (AMSs) sampling through pressure-controlled inlets

**Particulate emissions  
from Athabasca oil  
sands**

S. G. Howell et al.

Title Page

Abstract

Introduction

Conclusions

References

Tables

Figures

◀

▶

◀

▶

Back

Close

Full Screen / Esc

Printer-friendly Version

Interactive Discussion

(Bahreini et al., 2008) with vaporizers at 600 °C (DeCarlo et al., 2006). The P-3B AMS ran on an approximately 40% duty cycle, blanking 2 s, sampling for 2 s, and taking about a second to prepare for the next cycle. The DC-8 ran in so-called “fast mode” (Kimmel et al., 2011) with a duty cycle of about 75%. The measurements used here are bulk (not size-resolved)  $\text{SO}_4^-$ ,  $\text{NO}_3^-$ ,  $\text{NH}_4^+$  and non-refractory organic aerosol (OA) mass concentrations extracted using the publicly available Squirrel software (Allan et al., 2003, 2004; DeCarlo et al., 2006) and the collection efficiencies described in Middlebrook et al. (2012). It should be noted that the AMS has difficulty separating organosulphates from inorganic sulphate (Farmer et al., 2010). Black Carbon (BC) was measured with DMT Single Particle Soot Photometers (SP2s, Schwarz et al., 2006; Stephens et al., 2003). Unfortunately, the DC-8 SP2 was not operational on 10 July. The DC-8 had additional aerosol composition measurements, but at rates too slow to capture the oil sands plume.

The aerosol optics packages on both aircraft included TSI model 3563 nephelometers (Anderson et al., 1996) measuring light scattering  $B_{\text{sp}}$  at 450, 550, and 700 nm and Radiance Research Particle Soot Absorption Photometers (PSAPs) obtaining light absorption  $B_{\text{ap}}$  at 470, 530, and 660 nm. Nephelometer data were corrected for truncation errors using the procedures from Anderson and Ogren (1998). PSAP corrections were performed according to Virkkula et al. (2005) and Virkkula (2010).

As mentioned above, the DC-8 had an extensive set of trace gas measurements. Of particular interest here are CO,  $\text{SO}_2$ ,  $\text{NO}_2$ ,  $\text{NO}_x$ , and a suite of hydrocarbons and halocarbons collected in stainless steel chambers and measured with gas chromatography at UC Irvine. More extensive gas phase data are reported in Simpson et al. (2010).

The DC-8 was equipped with a Differential Absorption Lidar (DIAL, Browell et al., 1998; Dupont et al., 2012) which provides a 2-D curtain of backscatter data above and below the aircraft at 591 and 1064 nm. Data are presented here as attenuated aerosol backscatter ratio, defined as one less than the ratio of lidar return  $L$  to that calculated

for an atmosphere lacking aerosol  $L_m$ .

$$R_{ba} \equiv \frac{L}{L_m} - 1 = \frac{[\beta_p + \beta_m]}{\beta_m} (1 - \varepsilon_p)^2 - 1 \approx \frac{\beta_p}{\beta_m} \text{ if } \varepsilon_p \ll 1 \quad (1)$$

where  $\beta_p$  and  $\beta_m$  are backscattering due to particles and molecules (air) respectively, and  $\varepsilon_p$  is extinction along the beam due to particles. For the qualitative analysis here, this approximation is sufficient, but note that  $R_{ba}$  is an underestimate of the actual backscatter ratio when  $\varepsilon_p$  is significant, which often occurs when the DIAL penetrates thin clouds.

### 3 Results and discussion

The 10 July 2008 flights provide the bulk of our data. It was a clear day with broken low clouds and some higher clouds in the distance (Fig. 2). Surface winds below 1 km were from the SSW at 3 to 7  $\text{m s}^{-1}$  (near the climatological mean) but increased with altitude to 15  $\text{m s}^{-1}$  at 1 km and about 20  $\text{m s}^{-1}$  at 3.5 km. Above 1 km winds transitioned to about  $215 \pm 15^\circ$ . Convective activity and clouds were present in the area but no precipitation was evident. Some clouds interacted with emission plumes apparently mixing them to higher altitudes.

#### 3.1 Near-field characterization

The closest plume penetrations were too rapid for the PSAPs and size distributions, but the rapid-response measurements showed the plumes clearly (Fig. 4).  $\text{SO}_4^-$  and CO were found almost exclusively in the visible plumes from the tallest stacks. In contrast BC and OA appear to be produced in other locations as well, probably including the flaring stacks visible at the lower left in Fig. 2. Scattering and CN show both influences, dominated by the tall stacks but with other sources evident. This shows that

Title Page

Abstract

Introduction

Conclusions

References

Tables

Figures

◀

▶

◀

▶

Back

Close

Full Screen / Esc

Printer-friendly Version

Interactive Discussion





present in and between clouds during the descent (blue regions in Fig. 4). It is not clear how much of the sulphate in and around clouds was due to the well-known aqueous-phase reaction of  $\text{SO}_2$  with  $\text{H}_2\text{O}_2$  (Penkett et al., 1979). In this case the reaction is limited by the roughly 500 pptv concentration of  $\text{H}_2\text{O}_2$  seen by the DC-8, which could produce as much as  $2 \mu\text{g m}^{-3} \text{SO}_4^-$ . Reaction of  $\text{SO}_2$  with  $\text{NO}_2$  in cloud droplets could be a significant source of  $\text{SO}_4^-$  (Littlejohn et al., 1993; Sarwar et al., 2013), though this is a pH-dependent reaction that may be limited by available  $\text{NH}_3$  (which was not measured).

Figure 5 shows a similar dataset from the DC-8. At the 10 km distance of this sampling, the plume is more mixed, but some of the same features are visible. There is a double hump structure to many of the species. Given the winds and flight direction, the first peak would be from Suncor and the second from Syncrude. As with the P-3B,  $\text{SO}_4^-$  was found in a narrower region, indicating a couple of discrete sources.  $\text{SO}_2$  behaved similarly, while other species were more widely spread out.  $\text{NH}_4^+$  was also higher in the plume, but not sufficiently to neutralize the  $\text{SO}_4^-$ .  $\text{NH}_4^+:\text{SO}_4^-$  dropped from  $\sim 1.5$  in background air to 0.5 in the heart of the plume, indicating that  $\text{NH}_3$  was limited and the plume was acidic. Before the main plumes, from 18:25 to 18:28 UTC, scattering, absorption, OA, CO,  $\text{CO}_2$ , and CNhot were all moderately enhanced, due either to mining or the city of Ft. McMurray. In contrast,  $\text{NO}_2$  was quite low during that period.

Size distributions in the plume seen by the DC-8 are complex (Fig. 6). The APS (top panel) shows modes at  $3 \mu\text{m}$  at 18:30 and 18:32 UTC. That is typical for dust made mechanically and is likely to be road dust, from mining, or from crushing or mixing gravel. The  $1 \mu\text{m}$  mode around 18:31:40 UTC is more unusual – too small for mechanical generation and much larger than the typical accumulation mode of 0.1 to  $0.3 \mu\text{m}$  from gas to particle conversion. The latter is also seen in the UHSAS data at that time (bottom panel) at about  $0.6 \mu\text{m}$ . Since aerodynamic diameter as measured by the APS is related to geometric diameter by approximately the square root of density, this implies a particle density of at least  $2.8 \text{g cm}^{-3}$  (or higher, if the refractive index caused the UHSAS to oversize the particles). This is most likely to be fly ash, perhaps

## Particulate emissions from Athabasca oil sands

S. G. Howell et al.

Title Page

Abstract

Introduction

Conclusions

References

Tables

Figures

◀

▶

◀

▶

Back

Close

Full Screen / Esc

Printer-friendly Version

Interactive Discussion



from coke combustion (Barrie, 1980). Total and submicrometer light scattering is also plotted in the top panel. It is no surprise that coarse mode scattering is high during the dust events. However, maximum scattering occurred with the suspected fly ash, since 1  $\mu\text{m}$  particles are near the peak of mass scattering efficiency.

Figure 6 also reveals that near 18:30:30 UTC the 0.1 to 0.2  $\mu\text{m}$  accumulation mode caused 80 % of the scattering. This is coincident with the  $\text{SO}_4^{2-}$  and OA peaks from the AMS (Fig. 5). These sizes are very effective as CCN in BL clouds. CNhot, which typically consists mainly of BC and refractory organics (Clarke et al., 2007) is enhanced during the same period but also shows narrow peaks at other times (e.g. near 18:30 UTC). This is similar to those seen in the P3B data for stack emissions with high BC (Fig. 4). Consequently, the size distributions indicate different sources or processes embedded in the broad oil-sands plume contribute differently to both coarse and fine aerosol.

### 3.2 Vertical structure

Although aircraft have the ability to survey in 3 dimensions, in-situ measurements are limited to a 1-D line of observations along the flight track. A lidar curtain is an effective way to add a dimension, and thus context, to aerosol data. However, because aerosol size depends upon water uptake in response to relative humidity that generally varies with altitude (Shinozuka et al., 2011), the backscatter cannot directly quantify emitted dry aerosol mass. The DC-8 lidar had difficulty penetrating clouds in some spots, but did provide an overview of the plume (Fig. 7).

Figure 7b relates the lidar curtain and location of the plume to winds and geography. The wind vectors don't line up precisely with the 18:03 UTC start of the plume or maximum at 18:06 UTC as seen by the lidar, but small changes in wind direction are likely in the few hours it took the plume to reach the lidar track. The backscatter peak between 18:10 and 18:11 UTC is probably due to mining operations (see Fig. 1) but its magnitude is deceptive: the cloud at 4 km between 18:05 and 18:09 UTC suppresses the lower-altitude backscatter. The continued plume to 18:13:30 UTC is nearly

## Particulate emissions from Athabasca oil sands

S. G. Howell et al.

Title Page

Abstract

Introduction

Conclusions

References

Tables

Figures

◀

▶

◀

▶

Back

Close

Full Screen / Esc

Printer-friendly Version

Interactive Discussion



downwind of the city of Ft McMurray. Aerosol in the main plume appears to be mixed fairly uniformly to about 1450 m, but is drawn higher by convection around 18:05 UTC, presumably in a manner similar to that seen by the P-3B among clouds in Fig. 4.

### 3.3 Fluxes

- 5 One of the advantages of sampling from a mobile platform is that one can cross the entire plume and integrate a total flux if the vertical structure is known. The flux in the direction of the wind through the vertical projection of the flight track between times  $t_0$  and  $t_1$  is

$$Q = \int_{t_0}^{t_1} \int_0^{z_m} (S - S_0) v_w v_a \sin(\phi_a - \phi_w) dz dt \quad (2)$$

- 10 where  $z_m$  is the top of the boundary layer,  $S$  and  $S_0$  are the plume and background concentrations,  $v_a$  and  $\phi_a$  are aircraft speed and heading in Earth coordinates, and  $v_w$  and  $\phi_w$  are the wind speed and direction. If we assume winds and concentration are constant with altitude throughout the mixed layer and there is no vertical flux above the mixed layer then the discrete version of Eq. (2) becomes

$$15 \quad Q = z_m \sum_{t_0}^{t_1} (S - S_0) v_w v_a \sin(\phi_a - \phi_w) \Delta t \quad (3)$$

The flux from a source equals that through the flight path curtain if there are no significant sources or sinks along the way.

- The DC-8 loop around the two major upgraders is well suited to such a calculation. The upwind part of the loop provides the background concentrations (blue areas of Fig. 5) to subtract from the plume concentrations (brown). The primary difficulty and
- 20 major source of uncertainty is in establishing the mixed layer height  $z_m$ . The DC-8 did

## Particulate emissions from Athabasca oil sands

S. G. Howell et al.

Title Page

Abstract

Introduction

Conclusions

References

Tables

Figures

◀

▶

◀

▶

Back

Close

Full Screen / Esc

Printer-friendly Version

Interactive Discussion





**Particulate emissions  
from Athabasca oil  
sands**

S. G. Howell et al.

Title Page

Abstract

Introduction

Conclusions

References

Tables

Figures

◀

▶

◀

▶

Back

Close

Full Screen / Esc

Printer-friendly Version

Interactive Discussion



data, as both were about 10 km downwind. As seen in black in Fig. 9, the data, while scattered and a bit sparse, indicate MAE is roughly double that of the 10 July close pass. This amplification is as expected for particles with soot cores surrounded by non-absorbing coatings (Bond et al., 2006) and is similar to laboratory studies of coated soot (Schnaiter et al., 2005).

Table 2 enumerates most of the errors. “Instrument gaps” refers to how well the instrument can sample plume extremes. The AMS, for example, is blanking 25 % of the time so might miss peak concentrations. Convection out of the mixed layer is clearly visible in the lidar curtain (Fig. 7) between 18:04 and 18:06 UTC and by the P-3B when it is over 2.3 km (Fig. 4) but is sporadic and thus hard to quantify. Here we simply assume a maximum error caused by 25 % cloud cover with  $1 \text{ ms}^{-1}$  updrafts under those clouds exhausting mixed layer concentrations and returning zero concentration air between clouds. That would be sufficient to replace about half of the mixed layer in an hour. Dry deposition losses are not included because they are relatively small; even a deposition velocity of  $1 \text{ cm s}^{-1}$  would remove  $< 4\%$  of the column amount in the hour between emission and the DC-8 sampling.  $\text{NO}_2$  and  $\text{SO}_2$  also have photochemical sinks, but  $\leq 6\% \text{ h}^{-1}$  for  $\text{SO}_2$  (Cheng et al., 1987).

Environment Canada maintains a public website with historic emissions information. A search for  $\text{SO}_2$  emissions in 2008 reveals that the Syncrude and Suncor plants at Fort McMurray together released about  $1 \times 10^7 \text{ kg}$  in 2008, or  $3100 \text{ gs}^{-1}$ . Given our estimated errors and the questionable assumption that  $\text{SO}_2$  production on 10 July were representative of annual emissions, the combined  $\text{SO}_2$  and  $\text{SO}_4^-$  fluxes of  $4800 \text{ gs}^{-1}$  is excellent agreement.  $\text{NO}_y$  is even closer. The dramatic differences between reported and measured fluxes for CO are thus something of a surprise.  $\text{CO}_2$  fluxes were also higher than expected, but by a factor of 2.5. It may be that CO and  $\text{CO}_2$  production are more variable than  $\text{NO}_2$  and  $\text{SO}_2$  or that major sources were not included in the release inventories.

The largest uncertainties in the flux calculation are amenable to improvement with a more comprehensive flight plan. Multiple legs in the mixed layer and at higher alti-

tudes would permit better quantification of mixed layer uniformity, height, and exchange with air above. Perhaps most valuable would be a LIDAR curtain directly over the flux-measurement legs, which could address all of those at once.

Because they are unaffected by dilution, emission ratios can be determined with better precision than fluxes. Table 3 shows emission ratios of the aerosol species to CO from this work and from fresh forest fire plumes during ARCTAS. At the 10 km DC-8 distance from the source, emission ratios were similar for OA, but BC is enhanced in the oil sands plume about 3 times more and  $\text{SO}_4^-:\text{CO}$  is higher by a factor of 50. However, the average CO enhancement in the oil sands plume averaged 10.3 ppbv and peaked at 98 ppbv while forest fire peaked an order of magnitude higher, so OA in fire plumes often reached hundreds of  $\mu\text{g m}^{-3}$  (Cubison et al., 2011; Hecobian et al., 2011). Similarly, BC in the oil sands plume is small compared with even a single fire plume.

Comparisons between the oil sands plume and other aerosol sources suffer from some ambiguity, as results are strongly dependent on the time and space scales chosen. As an arbitrary example, Table 4 shows estimated annual emissions from forest fires throughout Canada from Amiro et al. (2009) in comparison to the oil sands fluxes from Table 1. On this scale the oil sands are an insignificant source of BC, OA, and CO (even though we found much higher CO than expected), but dwarf fire production of  $\text{SO}_2$ . Two caveats should be noted here: BC and OA have no precise chemical definition, so there are likely to be components of each that are primarily from the oil sands; and the fire season lasts only a couple of months, so aerosol from oil sands processing is certainly a more significant fraction of the total burden in other seasons.

### 3.4 Aerosol evolution

The P-3B and DC-8 flights near the sources on 7 July were the primary measurements for the oil-sands emissions. However, we also encountered the plume downwind at other times as shown in Fig. 3. These “encounters of opportunity” provide data to examine plume development over time and some evolution in gas and aerosol properties.

## Particulate emissions from Athabasca oil sands

S. G. Howell et al.

Title Page

Abstract

Introduction

Conclusions

References

Tables

Figures

◀

▶

◀

▶

Back

Close

Full Screen / Esc

Printer-friendly Version

Interactive Discussion



**Particulate emissions  
from Athabasca oil  
sands**

S. G. Howell et al.

Title Page

Abstract

Introduction

Conclusions

References

Tables

Figures

◀

▶

◀

▶

Back

Close

Full Screen / Esc

Printer-friendly Version

Interactive Discussion



Figure 10 shows P-3B data for the 29 June and 28 June flight segments, about 10 and 180 km downwind of the upgraders. Unfortunately, on 29 June, the CO went through a calibration cycle at exactly the peak of the plume. The  $\text{SO}_4^-$  peak that day was much smaller than on 10 July, indicating that the plane may have missed the main part of the plume or that  $\text{SO}_2$  production was lower that day. As with the DC-8 data discussed above and collected at roughly the same distance, the plume in Fig. 10a is complex, indicating a variety of sources. OA appears to have a much higher background, perhaps of biogenic origin as BC was low. A broad plume with dust and organic aerosol from 22:38 to 22:40 UTC may correspond to mining operations and the evaporative plume from Simpson et al. (2010). The enhanced  $\text{SO}_4^-$  and very large UCN around 22:42 UTC indicate the upgrader plume. As with the 10 July data, most of the particles are volatile, so are not detected as CNhot. A review of the forward video reveals that the very narrow peak at 22:43:39 UTC occurred shortly after the plane flew over a road where trucks could be seen raising clouds of dust. Dust was responsible for much of the light scattering seen throughout the plume crossing; the very similar patterns at all wavelengths can only occur with particles large compared to the wavelength. While  $\text{SO}_4^-$  was far smaller than that seen by the DC-8 a similar distance away, the dust seen by the APS was similar, though the  $1\ \mu\text{m}$  mode was absent, further evidence that the plane either missed part of the plume or that the industrial facilities were operating differently.

In contrast to the detail visible at 10 km, the plume at 180 km downwind (Fig. 10b) is broad and smooth. Wind speeds were about  $10\ \text{m s}^{-1}$ , so the plume was about 5 h old. The dust is no longer obvious, presumably diluted, as dry deposition time scales are likely to be about 12 h for  $5\ \mu\text{m}$  particles, which have a deposition velocity of roughly  $2\ \text{cm s}^{-1}$  in coniferous forests with that wind speed (Zhang et al., 2001). However, the roughly  $1\ \mu\text{m}$  possible fly ash mode is evident. The disparity between the red and blue channels reveals that small particles now dominate the scattering. While overall particle concentrations are lower (note the log scales on the CN data), there are now very few volatile particles, and higher CNhot suggests that at least some of the secondary

organic material in the aerosol has low volatility. Once again,  $\text{SO}_4^-$  and OA are well correlated. CO, which is stable at these time scales, rises about 6 ppbv.

Flux calculations like those in Sect. 3.3 can be applied here, though errors are even more poorly quantified: the mixed layer top of 2900 m is solely from a descent prior to the plume crossing; the P-3B wind speeds were compromised by the radiometer on the nose of the aircraft; and the end time of the plume is rather ambiguous. Thus, these fluxes are just rough approximations. Table 1 shows the range of fluxes calculated for reasonable definitions of the end of the plume. Values for  $\text{SO}_4^-$  and OA do not change much in this calculation, while BC and CO are sensitive to the plume duration and are particularly uncertain.

While very approximate, the fluxes calculated in this flyby do confirm the high CO emissions from the DC-8 loop. The increased  $\text{SO}_4^-$  : CO is as expected, since sulphate production from  $\text{SO}_2$  continues while CO is inert at these time scales. If  $\text{SO}_2$  emissions were the same those two days, then the additional 320 to 370  $\text{gs}^{-1}$  represents about 8% of the  $\text{SO}_2$  in the roughly 5 h since emission, still more than can be attributed to reaction with 0.1 pptv OH.

The correlation between OA and  $\text{SO}_4^-$  at 10 and 180 km and during the P3-B downwind leg reinforce the idea that  $\text{SO}_4^-$  production governs secondary OA formation through either acid-catalyzed polymerization or organosulfate production. The relative isolation of the oil sands plume and its high acidity may provide an excellent opportunity to study these reactions outside of a laboratory environment.

The increased small particle scattering in Fig. 10b is due to growth of particles initially too small to affect visible light. This is revealed by comparing DMA distributions obtained in each plume. In Fig. 11 we compare number distributions measured near the source (10 km downwind, black) with several distributions measured at 172 to 192 km downwind (red). The mean of the latter (heavy dashed red) has a peak near 0.06  $\mu\text{m}$  compared to 0.015  $\mu\text{m}$  near the source. This indicates that some sizes near the source were too small to be active as CCN in BL clouds but have grown to be effective CCN (i.e. larger than about 0.06  $\mu\text{m}$ ) downwind for low clouds. Corresponding growth in the

## Particulate emissions from Athabasca oil sands

S. G. Howell et al.

Title Page

Abstract

Introduction

Conclusions

References

Tables

Figures

◀

▶

◀

▶

Back

Close

Full Screen / Esc

Printer-friendly Version

Interactive Discussion



larger mode near 0.1  $\mu\text{m}$  is also evident but as most in this mode were also larger than 0.06  $\mu\text{m}$  before aging, this growth strongly affects light scattering but has only a second order effect on their effectiveness as CCN.

As shown in Fig. 3, the DC-8 also intercepted the plume on 29 June. It was inadvertent; the plan was to sample a fire plume seen the previous day. The low-altitude sampling leg was cut short when no smoke was found. However, elevated  $\text{SO}_2$  and  $\text{NO}_y$  suggest the oil sands plume was present Fig. 12. A variety of hydrocarbons were also detected, consistent with those identified in the oil sands plume by Simpson et al. (2010). This was not a forest fire plume—CO was only slightly enriched and other biomass indicators like HCN were not elevated at all. The gas ratios did not resemble those identified in the Simpson et al. (2011) analysis of boreal forest fire plumes.

Low-altitude winds and back trajectories are consistent with transport from the Ft. McMurray area (Fig. 13). Trajectories from the southern end of the leg did pass directly over the upgraders about 5 h earlier, but at an altitude 1400 m above the facilities. Low altitude winds evidently carried the plume north for a few hours before lofting it to 900 m, where the back trajectories led to the northern end of the flight leg.

However, the aerosol signature usually present in the oil sands plume were weak. CN and scattering rose only slightly. More surprisingly, while AMS OA correlated well with  $\text{SO}_2$ ,  $\text{NO}_y$ , and organic vapors, the OA :  $\text{SO}_4^-$  ratio was 8 : 1 rather than 1 : 1. This suggests some removal mechanism, rather than simply dilution, was active. Rain was reported at Ft. McMurray at 02:00 and 03:00 LT (09:00 and 10:00 UTC) on the 29th (Environment Canada, 2008b), about 7 h before the DC-8 flight. One likely explanation is that much of the  $\text{SO}_2$  reacted in cloud to form  $\text{SO}_4^-$ , which was effectively removed by rain, while leaving insoluble organic vapors unaffected. Photochemical reactions after sunrise could then produce the organic aerosol seen in Fig. 12.

## Particulate emissions from Athabasca oil sands

S. G. Howell et al.

Title Page

Abstract

Introduction

Conclusions

References

Tables

Figures

◀

▶

◀

▶

Back

Close

Full Screen / Esc

Printer-friendly Version

Interactive Discussion



## 4 Conclusions

While 2 flybys and 3 incidental plume penetrations can only provide short-term estimates of the aerosol output of the Alberta oil sands mining and upgrading operations, these flights have established that emissions fluxes can be measured, at least under favorable weather conditions, but with uncertainties of about a factor of 2. The primary sources of error are mixed layer depth and homogeneity and exchange with overlying air. Careful flight planning, extended sampling including multiple altitudes, and LIDAR data along the flux cross section could greatly enhance the accuracy of the flux calculations, probably to within 50 %.

SO<sub>2</sub> and NO<sub>2</sub> emission inventories lie within error estimates of our calculated flux, though our measurements of CO fluxes substantially exceeded reported emissions during two plume penetrations. CO<sub>2</sub> emissions were also above reported emissions, but not by a large factor. Black carbon fluxes are highly uncertain, but appear to be roughly 10 gs<sup>-1</sup>.

While neither the mining operations nor the industrial facilities produce much particulate organic matter directly, organic aerosol appears rapidly within the industrial plume in a short time, creating particulate mass approximately equal to the sulphate. Some of this may be primary OA, due to condensation of vapors as the plume cools, but reactions between H<sub>2</sub>SO<sub>4</sub> and either biogenic or plume-derived organic vapors appear to be important. At least over short ranges, we confirm the SO<sub>2</sub> photochemical loss rates from Cheng et al. (1987), though reaction with OH appears insufficient to account for the conversion rate to SO<sub>4</sub><sup>=</sup>.

The industrial plume has tremendously high aerosol number concentrations, saturating our counting instruments, but those particles are too small to scatter light or serve as effective CCN. They do coagulate and grow, so by the time the plume is a few hours old, CCN concentrations and scattering are affected. Major light scattering components of the aerosol are the accumulation mode in the industrial plume, dust, and what appears to be fly ash.

### Particulate emissions from Athabasca oil sands

S. G. Howell et al.

Title Page

Abstract

Introduction

Conclusions

References

Tables

Figures

◀

▶

◀

▶

Back

Close

Full Screen / Esc

Printer-friendly Version

Interactive Discussion





## Particulate emissions from Athabasca oil sands

S. G. Howell et al.

Title Page

Abstract

Introduction

Conclusions

References

Tables

Figures

◀

▶

◀

▶

Back

Close

Full Screen / Esc

Printer-friendly Version

Interactive Discussion

interpretation and error analysis, *J. Geophys. Res.*, 108, 4090, doi:10.1029/2002JD002358, 2003. 21307

Allan, J. D., Delia, A. E., Coe, H., Bower, K. N., Alfarra, M., Jimenez, J. L., Middlebrook, A. M., Drewnick, F., Onasch, T. B., Canagaratna, M. R., Jayne, J. T., and Worsnop, D. R.: A generalised method for the extraction of chemically resolved mass spectra from Aerodyne aerosol mass spectrometer data, *J. Aerosol. Sci.*, 35, 909–922, doi:10.1016/j.jaerosci.2004.02.007, 2004. 21307

Amiro, B., Cantin, A., Flannigan, M., and de Groot, W.: Future emissions from Canadian boreal forest fires, *Can. J. Forest. Res.*, 39, 383–395, doi:10.1139/X08-154, 2009. 21315, 21330

Anderson, T. L. and Ogren, J. A.: Determining aerosol radiative properties using the TSI 3563 integrating nephelometer, *Aerosol Sci. Tech.*, 29, 57–69, doi:10.1080/02786829808965551, 1998. 21307

Anderson, T., Covert, D., Marshall, S., Laucks, M., Charlson, R., Waggoner, A., Ogren, J., Caldwell, R., Holm, R., Quant, F., Sem, G., Wiedensohler, A., Ahlquist, N., and Bates, T.: Performance characteristics of a high-sensitivity, three-wavelength, total scatter/backscatter nephelometer, *J. Atmos. Ocean. Tech.*, 13, 967–986, doi:10.1175/1520-0426(1996)013<0967:PCOAHS>2.0.CO;2, 1996. 21307

Bahreini, R., Dunlea, E., Matthew, B., Simons, C., Docherty, K., DeCarlo, P., Jimenez, J., Brock, C., and Middlebrook, A.: Design and operation of a pressure controlled inlet for airborne sampling with an aerodynamic aerosol lens, *Aerosol Sci. Tech.*, 42, 465–471, 2008. 21307

Baron, P. and Willeke, K.: *Aerosol Measurement: Principles, Techniques, and Applications*, Wiley, New York, 2001. 21306

Barrie, L.: The fate of particulate emissions from an isolated power plant in the oil sands area of Western Canada, *Ann. NY Acad. Sci.*, 338, 434–452, 1980. 21303, 21304, 21311

Blitz, M. A., Hughes, K. J., and Pilling, M. J.: Determination of the high-pressure limiting rate coefficient and the enthalpy of reaction for OH + SO<sub>2</sub>, *J. Phys. Chem. A*, 107, 1971–1978, doi:10.1021/jp026524y, 2003. 21313

Bond, T. C. and Bergstrom, R. W.: Light absorption by carbonaceous particles: an investigative review, *Aerosol Sci. Tech.*, 40, 27–67, doi:10.1080/02786820500421521, 2006. 21313

Bond, T., Habib, G., and Bergstrom, R.: Limitations in the enhancement of visible light absorption due to mixing state, *J. Geophys. Res.*, 111, D20211, doi:10.1029/2006JD007315, 2006. 21314



**Particulate emissions  
from Athabasca oil  
sands**

S. G. Howell et al.

Title Page

Abstract

Introduction

Conclusions

References

Tables

Figures

◀

▶

◀

▶

Back

Close

Full Screen / Esc

Printer-friendly Version

Interactive Discussion



Browell, E., Ismail, S., and Grant, W.: Differential absorption lidar (DIAL) measurements from air and space, *Appl. Phys. B-Lasers O.*, 67, 399–410, doi:10.1007/s003400050523, 1998. 21307

Cheng, L., Peake, E., and Davis, A.: The rate of SO<sub>2</sub> to sulfate particle formation in an air parcel from an oil sands extraction plant plume, *JAPCA J. Air Waste Ma.*, 37, 163–167, doi:10.1080/08940630.1987.10466211, 1987. 21303, 21304, 21313, 21314, 21319

Clarke, A., McNaughton, C., Kapustin, V., Shinozuka, Y., Howell, S., Dibb, J., Zhou, J., Anderson, B., Brekhovskikh, V., Turner, H., and Pinkerton, M.: Biomass burning and pollution aerosol over North America: organic components and their influence on spectral optical properties and humidification response, *J. Geophys. Res.*, 112, D12S18, doi:10.1029/2006JD007777, 2007. 21311

Clarke, A. D.: A thermo-optic technique for in situ analysis of size-resolved aerosol physico-chemistry, *Atmos. Environ.*, 25A, 635–644, 1991. 21306

Cubison, M. J., Ortega, A. M., Hayes, P. L., Farmer, D. K., Day, D., Lechner, M. J., Brune, W. H., Apel, E., Diskin, G. S., Fisher, J. A., Fuelberg, H. E., Hecobian, A., Knapp, D. J., Mikoviny, T., Riemer, D., Sachse, G. W., Sessions, W., Weber, R. J., Weinheimer, A. J., Wisthaler, A., and Jimenez, J. L.: Effects of aging on organic aerosol from open biomass burning smoke in aircraft and laboratory studies, *Atmos. Chem. Phys.*, 11, 12049–12064, doi:10.5194/acp-11-12049-2011, 2011. 21315

Davies, M.: Air quality modeling in the Athabasca oil sands region, in: *Alberta Oil Sands*, chap. 12, *Developments in Environmental Science*, vol. 11, edited by: Percy, K. E., Elsevier, 267–309, doi:10.1016/B978-0-08-097760-7.00012-3, 2012. 21304

DeCarlo, P., Kimmel, J., Trimborn, A., Northway, M., Jayne, J., Aiken, A., Gonin, M., Fuhrer, K., Horvath, T., Docherty, K., Worsnop, D. R., and Jimenez, J. L.: Field-deployable, high-resolution, time-of-flight aerosol mass spectrometer, *Anal. Chem.*, 78, 8281–8289, doi:10.1021/ac061249n, 2006. 21307

Dupont, R., Pierce, B., Worden, J., Hair, J., Fenn, M., Hamer, P., Natarajan, M., Schaack, T., Lenzen, A., Apel, E., Dibb, J., Diskin, G., Huey, G., Weinheimer, A., Kondo, Y., and Knapp, D.: Attribution and evolution of ozone from Asian wild fires using satellite and aircraft measurements during the ARCTAS campaign, *Atmos. Chem. Phys.*, 12, 169–188, doi:10.5194/acp-12-169-2012, 2012. 21307

## Particulate emissions from Athabasca oil sands

S. G. Howell et al.

Title Page

Abstract

Introduction

Conclusions

References

Tables

Figures

◀

▶

◀

▶

Back

Close

Full Screen / Esc

Printer-friendly Version

Interactive Discussion



Environment Canada: National Pollutant Release Inventory Facility Data Search-Alberta Oil-sands and Heavy Oil, available at: [http://www.ec.gc.ca/pdb/websol/querysite/query\\_e.cfm](http://www.ec.gc.ca/pdb/websol/querysite/query_e.cfm) (last access: October 2012), 2008a. 21327

Environment Canada: National Climate Data and Information Archive, available at: [http://www.climate.weatheroffice.gc.ca/climateData/hourlydata\\_e.html?timeframe=1&Prov=ALTA&StationID=2519&hlyRange=1953-01-01\\$1\\$2008-09-25&Year=2008&Month=6&Day=29](http://www.climate.weatheroffice.gc.ca/climateData/hourlydata_e.html?timeframe=1&Prov=ALTA&StationID=2519&hlyRange=1953-01-01$1$2008-09-25&Year=2008&Month=6&Day=29) (last access: October 2012), 2008b. 21318

Farmer, D. K., Matsunaga, A., Docherty, K. S., Surratt, J. D., Seinfeld, J. H., Ziemann, P. J., and Jimenez, J. L.: Response of an aerosol mass spectrometer to organonitrates and organosulfates and implications for atmospheric chemistry, *P. Natl. Acad. Sci. USA*, 107, 6670–6675, doi:10.1073/pnas.0912340107, 2010. 21307

Fuller, K. A., Malm, W. C., and Kreidenweis, S. M.: Effects of mixing on extinction by carbonaceous particles, *J. Geophys. Res.*, 104, 15941–15954, doi:10.1029/1998JD100069, 1999. 21313

Hecobian, A., Liu, Z., Hennigan, C. J., Huey, L. G., Jimenez, J. L., Cubison, M. J., Vay, S., Diskin, G. S., Sachse, G. W., Wisthaler, A., Mikoviny, T., Weinheimer, A. J., Liao, J., Knapp, D. J., Wennberg, P. O., Kürten, A., Crouse, J. D., Clair, J. St., Wang, Y., and Weber, R. J.: Comparison of chemical characteristics of 495 biomass burning plumes intercepted by the NASA DC-8 aircraft during the ARCTAS/CARB-2008 field campaign, *Atmos. Chem. Phys.*, 11, 13325–13337, doi:10.5194/acp-11-13325-2011, 2011. 21315

Jacob, D. J., Crawford, J. H., Maring, H., Clarke, A. D., Dibb, J. E., Emmons, L. K., Ferrare, R. A., Hostetler, C. A., Russell, P. B., Singh, H. B., Thompson, A. M., Shaw, G. E., McCauley, E., Pederson, J. R., and Fisher, J. A.: The Arctic Research of the Composition of the Troposphere from Aircraft and Satellites (ARCTAS) mission: design, execution, and first results, *Atmos. Chem. Phys.*, 10, 5191–5212, doi:10.5194/acp-10-5191-2010, 2010. 21304

Jang, M., Czoschke, N. M., Lee, S., and Kamens, R. M.: Heterogeneous atmospheric aerosol production by acid-catalyzed particle-phase reactions, *Science*, 298, 814–817, doi:10.1126/science.1075798, 2002. 21309

Kimmel, J. R., Farmer, D. K., Cubison, M. J., Sueper, D., Tanner, C., Nemitz, E., Worsnop, D. R., Gonin, M., and Jimenez, J. L.: Real-time aerosol mass spectrometry with millisecond resolution, *Int. J. Mass. Spectrom.*, 303, 15–26, doi:10.1016/j.ijms.2010.12.004, 2011. 21307

Littlejohn, D., Wang, Y., and Chang, S. G.: Oxidation of aqueous sulfite ion by nitrogen dioxide, *Environ. Sci. Technol.*, 27, 2162–2167, doi:10.1021/es00047a024, 1993. 21310

**Particulate emissions  
from Athabasca oil  
sands**

S. G. Howell et al.

Title Page

Abstract

Introduction

Conclusions

References

Tables

Figures

◀

▶

◀

▶

Back

Close

Full Screen / Esc

Printer-friendly Version

Interactive Discussion



McLinden, C. A., Fioletov, V., Boersma, K. F., Krotkov, N., Sioris, C. E., Veefkind, J. P., and Yang, K.: Air quality over the Canadian oil sands: a first assessment using satellite observations, *Geophys. Res. Lett.*, 39, L04804, doi:10.1029/2011GL050273, 2012. 21304

McNaughton, C. S., Clarke, A. D., Howell, S. G., Pinkerton, M., Anderson, B., Thornhill, L., Winstead, E., Hudgins, C., Dibb, J. E., Scheuer, E., and Maring, H.: Results from the DC-8 inlet characterization experiment (DICE): airborne vs. surface sampling of mineral dust and sea salt aerosols, *Aerosol Sci. Tech.*, 41, 136–159, doi:10.1080/02786820601118406, 2007. 21305

Middlebrook, A. M., Bahreini, R., Jimenez, J. L., and Canagaratna, M. R.: Evaluation of composition-dependent collection efficiencies for the aerodyne aerosol mass spectrometer using field data, *Aerosol Sci. Tech.*, 46, 258–271, doi:10.1080/02786826.2011.620041, 2012. 21307

Ng, N. L., Canagaratna, M. R., Jimenez, J. L., Zhang, Q., Ulbrich, I. M., and Worsnop, D. R.: Real-time methods for estimating organic component mass concentrations from aerosol mass spectrometer data, *Environ. Sci. Technol.*, 45, 910–916, doi:10.1021/es102951k, 2011. 21309

Penkett, S., Jones, B., Brich, K., and Eggleton, A.: The importance of atmospheric ozone and hydrogen peroxide in oxidising sulphur dioxide in cloud and rainwater, *Atmos. Environ.*, 13, 123–137, doi:10.1016/0004-6981(79)90251-8, 1979. 21310

Proemse, B. C., Mayer, B., Chow, J. C., and Watson, J. G.: Isotopic characterization of nitrate, ammonium and sulfate in stack PM<sub>2.5</sub> emissions in the Athabasca oil sands region, Alberta, Canada, *Atmos. Environ.*, 60, 555–563, doi:10.1016/j.atmosenv.2012.06.046, 2012a. 21304

Proemse, B. C., Mayer, B., and Fenn, M. E.: Tracing industrial sulfur contributions to atmospheric sulfate deposition in the Athabasca oil sands region, Alberta, Canada, *Appl. Geochem.*, 27, 2425–2434, doi:10.1016/j.apgeochem.2012.08.006, 2012b. 21304

Sarwar, G., Fahey, K., Kwok, R., Gilliam, R. C., Roselle, S. J., Mathur, R., Xue, J., Yu, J., and Carter, W. P.: Potential impacts of two SO<sub>2</sub> oxidation pathways on regional sulfate concentrations: aqueous-phase oxidation by NO<sub>2</sub> and gas-phase oxidation by stabilized Criegee intermediates, *Atmos. Environ.*, 68, 186–197, doi:10.1016/j.atmosenv.2012.11.036, 2013. 21310

Schnaiter, M., Linke, C., Möhler, O., Naumann, K. H., Saathoff, H., Wagner, R., Schurath, U., and Wehner, B.: Absorption amplification of black carbon internally mixed with secondary organic aerosol, *J. Geophys. Res.*, 110, D19204, doi:10.1029/2005JD006046, 2005. 21314

**Particulate emissions  
from Athabasca oil  
sands**

S. G. Howell et al.

Title Page

Abstract

Introduction

Conclusions

References

Tables

Figures

◀

▶

◀

▶

Back

Close

Full Screen / Esc

Printer-friendly Version

Interactive Discussion

- Schwarz, J. P., Gao, R. S., Fahey, D. W., Thomson, D. S., Watts, L. A., Wilson, J. C., Reeves, J. M., Darbeheshti, M., Baumgardner, D. G., Kok, G. L., Chung, S. H., Schulz, M., Hendricks, J., Lauer, A., Kärcher, B., Slowik, J. G., Rosenlof, K. H., Thompson, T. L., Langford, A. O., Loewenstein, M., and Aikin, K. C.: Single-particle measurements of midlatitude black carbon and light-scattering aerosols from the boundary layer to the lower stratosphere, *J. Geophys. Res.*, 111, D16207, doi:10.1029/2006JD007076, 2006. 21307
- Shinozuka, Y., Redemann, J., Livingston, J. M., Russell, P. B., Clarke, A. D., Howell, S. G., Freitag, S., O'Neill, N. T., Reid, E. A., Johnson, R., Ramachandran, S., McNaughton, C. S., Kapustin, V. N., Brekhovskikh, V., Holben, B. N., and McArthur, L. J. B.: Airborne observation of aerosol optical depth during ARCTAS: vertical profiles, inter-comparison and fine-mode fraction, *Atmos. Chem. Phys.*, 11, 3673–3688, doi:10.5194/acp-11-3673-2011, 2011. 21311
- Simpson, I. J., Blake, N. J., Barletta, B., Diskin, G. S., Fuelberg, H. E., Gorham, K., Huey, L. G., Meinardi, S., Rowland, F. S., Vay, S. A., Weinheimer, A. J., Yang, M., and Blake, D. R.: Characterization of trace gases measured over Alberta oil sands mining operations: 76 speciated C<sub>2</sub>–C<sub>10</sub> volatile organic compounds (VOCs), CO<sub>2</sub>, CH<sub>4</sub>, CO, NO, NO<sub>2</sub>, NO<sub>y</sub>, O<sub>3</sub> and SO<sub>2</sub>, *Atmos. Chem. Phys.*, 10, 11931–11954, doi:10.5194/acp-10-11931-2010, 2010. 21304, 21307, 21309, 21316, 21318
- Simpson, I. J., Akagi, S. K., Barletta, B., Blake, N. J., Choi, Y., Diskin, G. S., Fried, A., Fuelberg, H. E., Meinardi, S., Rowland, F. S., Vay, S. A., Weinheimer, A. J., Wennberg, P. O., Wiebring, P., Wisthaler, A., Yang, M., Yokelson, R. J., and Blake, D. R.: Boreal forest fire emissions in fresh Canadian smoke plumes: C<sub>1</sub>–C<sub>10</sub> volatile organic compounds (VOCs), CO<sub>2</sub>, CO, NO<sub>2</sub>, NO, HCN and CH<sub>3</sub>CN, *Atmos. Chem. Phys.*, 11, 6445–6463, doi:10.5194/acp-11-6445-2011, 2011. 21318
- Singh, H., Anderson, B., Brune, W., Cai, C., Cohen, R., Crawford, J., Cubison, M., Czech, E., Emmons, L., Fuelberg, H., Huey, G., Jacob, D., Jimenez, J., Kaduwela, A., Kondo, Y., Mao, J., Olson, J., Sachse, G., Vay, S., Weinheimer, A., Wennberg, P., and Wisthaler, A.: Pollution influences on atmospheric composition and chemistry at high northern latitudes: boreal and California forest fire emissions, *Atmos. Environ.*, 44, 4553–4564, doi:10.1016/j.atmosenv.2010.08.026, 2010. 21329
- Stephens, M., Turner, N., and Sandberg, J.: Particle identification by laser-induced incandescence in a solid-state laser cavity, *Appl. Optics*, 42, 3726–3736, doi:10.1364/AO.42.003726, 2003. 21307

**Particulate emissions  
from Athabasca oil  
sands**

S. G. Howell et al.

Title Page

Abstract

Introduction

Conclusions

References

Tables

Figures

◀

▶

◀

▶

Back

Close

Full Screen / Esc

Printer-friendly Version

Interactive Discussion



Strausz, O., Jha, K. N., and Montgomery, D. S.: Chemical composition of gases in Athabasca bitumen and in low-temperature thermolysis of oil sand, asphaltene and maltene, *Fuel*, 56, 114–120, doi:10.1016/0016-2361(77)90128-4, 1977. 21303

5 Surratt, J. D., Lewandowski, M., Offenberg, J. H., Jaoui, M., Kleindienst, T. E., Edney, E. O., and Seinfeld, J. H.: Effect of acidity on secondary organic aerosol formation from isoprene, *Environ. Sci. Technol.*, 41, 5363–5369, doi:10.1021/es0704176, 2007. 21309

Virkkula, A.: Correction of the Calibration of the 3-wavelength particle soot absorption photometer (3 $\lambda$  PSAP), *Aerosol Sci. Tech.*, 44, 706–712, doi:10.1080/02786826.2010.482110, 2010. 21307

10 Virkkula, A., Ahlquist, N., Covert, D., Arnott, W., Sheridan, P., Quinn, P., and Coffman, D.: Modification, calibration and a field test of an instrument for measuring light absorption by particles, *Aerosol Sci. Tech.*, 39, 68–83, 2005. 21307

Zhang, H., Worton, D. R., Lewandowski, M., Ortega, J., Rubitschun, C. L., Park, J.-H., Kristensen, K., Campuzano-Jost, P., Day, D. A., Jimenez, J. L., Jaoui, M., Offenberg, J. H., Kleindienst, T. E., Gilman, J., Kuster, W. C., de Gouw, J., Park, C., Schade, G. W., Frossard, A. A., Russell, L., Kaser, L., Jud, W., Hansel, A., Cappellin, L., Karl, T., Glasius, M., Guenther, A., Goldstein, A. H., Seinfeld, J. H., Gold, A., Kamens, R. M., and Surratt, J. D.: Organosulfates as tracers for Secondary Organic Aerosol (SOA) formation from 2-Methyl-3-Buten-2-ol (MBO) in the atmosphere, *Environ. Sci. Technol.*, 46, 9437–9446, doi:10.1021/es301648z, 2012. 21309

20 Zhang, L., Gong, S., Padro, J., and Barrie, L.: A size-segregated particle dry deposition scheme for an atmospheric aerosol module, *Atmos. Environ.*, 35, 549–560, doi:10.1016/S1352-2310(00)00326-5, 2001. 21316

## Particulate emissions from Athabasca oil sands

S. G. Howell et al.

**Table 1.** Fluxes calculated from the DC-8 loop around the oil sands facilities on 10 July and the P3-B plume penetration on 28 June. Estimated errors are roughly a factor of 2 for the DC-8 flyby (Table 2) and higher for the P3-B. The latter column includes a range of values since the plume with is ambiguous. See text and Fig. 10b. “Reported” values are from Environment Canada (2008a) and the Greenhouse Gas Inventory (for CO<sub>2</sub>), reporting year 2008. All sources within the DC-8 loop are included, though the Syncrude and Suncor upgraders are by far the largest.

Species	Flux, gs <sup>-1</sup>		Reported
	DC-8, 10 km	P3-B, 180 km	
NO <sub>2</sub> (NCAR)	440		
NO <sub>y</sub> (as NO <sub>2</sub> )	910		730
SO <sub>2</sub> (GA Tech)	4500		
AMS SO <sub>4</sub> <sup>-</sup>	280	600–650	
SO <sub>2</sub> + SO <sub>4</sub> <sup>-</sup>	4800		3100
AMS OA	260	550–750	
AMS total	600		
BC (from PSAP)	9	0.5–5	
CO	2100	1800–4000	290
CO <sub>2</sub>	1 700 000		640 000

[Title Page](#)
[Abstract](#)
[Introduction](#)
[Conclusions](#)
[References](#)
[Tables](#)
[Figures](#)
[Back](#)
[Close](#)
[Full Screen / Esc](#)
[Printer-friendly Version](#)
[Interactive Discussion](#)


## Particulate emissions from Athabasca oil sands

S. G. Howell et al.

**Table 2.** Flux error estimates.

Error	AMS	BC	NO <sub>2</sub>	SO <sub>2</sub>	CO	CO <sub>2</sub>
Instrument accuracy	35 %	50 %	10 %	10 %	2 %	0.1 %
Clean/plume difference	5 %	5 %	5 %	2 %	20 %	5 %
Instrument gaps	5 %	0 %	5 %	0 %	0 %	5 %
Mixed layer height			50 %			
Mixed layer uniformity			30 % (from lidar)			
Wind speed			Assume 30 %			
Loss from mixed layer			+50 %, -0 %			
TOTAL	+90 % -75 %	+95 % -85 %	+85 % -70 %	+85 % -65 %	+85 % -70 %	+85 % -65 %

[Title Page](#)
[Abstract](#)
[Introduction](#)
[Conclusions](#)
[References](#)
[Tables](#)
[Figures](#)
[◀](#)
[▶](#)
[◀](#)
[▶](#)
[Back](#)
[Close](#)
[Full Screen / Esc](#)
[Printer-friendly Version](#)
[Interactive Discussion](#)


**Particulate emissions  
from Athabasca oil  
sands**

S. G. Howell et al.

Title Page

Abstract

Introduction

Conclusions

References

Tables

Figures

◀

▶

◀

▶

Back

Close

Full Screen / Esc

Printer-friendly Version

Interactive Discussion



**Table 3.** Aerosol enhancement ratios relative to CO. Units are mg aerosol (gCO)<sup>-1</sup>. Forest fire data are from fresh plumes observed during ARCTAS (Singh et al., 2010).

Species	Oil sands	Forest fires
OA	120 ± 60	120 ± 50
SO <sub>4</sub> <sup>=</sup>	130 ± 60	2.4 ± 1.4
BC	4.3 ± 2.3	1.6 ± 0.9

## Particulate emissions from Athabasca oil sands

S. G. Howell et al.

Title Page

Abstract

Introduction

Conclusions

References

Tables

Figures

◀

▶

◀

▶

Back

Close

Full Screen / Esc

Printer-friendly Version

Interactive Discussion



**Table 4.** Emissions from the oil sands in comparison to estimated forest fire production. BC, NO<sub>y</sub>, and CO are directly from Amiro et al. (2009) while the others use ratios to CO during fire plume penetrations in ARCTAS (as identified by acetonitrile > 0.5 ppbv). Units are Ggyr<sup>-1</sup>. The SO<sub>4</sub><sup>-</sup> numbers are a bit misleading, as some of the SO<sub>2</sub> will react to create more sulphate.

Species	Oil sands	Forest fires	OS : FF
BC	0.3	34	1 %
NO <sub>y</sub>	29	181	16 %
CO	66	6450	1 %
SO <sub>4</sub> <sup>-</sup>	9	13	70 %
SO <sub>2</sub>	140	13	1000 %
OA	8	900	1 %



**Fig. 1.** Imagery of the oil sands region from 29 June and flight tracks from 10 July. The DC-8 track is blue; the P3B, red. The two planes entered the area from the north along the parallel tracks to the right. The DC-8 then looped counterclockwise around the facilities at about 350 m a.g.l. 90 min later the P-3B approached from the south and flew the figure 8 shown, penetrating the Syncrude facility plume three times, twice at about 250 m a.g.l. and once at 600 m. The Suncor upgrader plume was sampled once, at 250 m.

**Particulate emissions from Athabasca oil sands**

S. G. Howell et al.

Title Page	
Abstract	Introduction
Conclusions	References
Tables	Figures
◀	▶
◀	▶
Back	Close
Full Screen / Esc	
Printer-friendly Version	
Interactive Discussion	





**Fig. 2.** The Suncor facility about 12 s before the P-3B encountered the white/gray plume. Stacks emitting darker plumes are visible to the left. The Athabasca river, settling ponds, and mined areas are visible in the background. The image is a still from a windshield-mounted video camera.

Particulate emissions from Athabasca oil sands

S. G. Howell et al.

Title Page

Abstract Introduction

Conclusions References

Tables Figures

⏪ ⏩

◀ ▶

Back Close

Full Screen / Esc

Printer-friendly Version

Interactive Discussion



**Particulate emissions  
from Athabasca oil  
sands**

S. G. Howell et al.

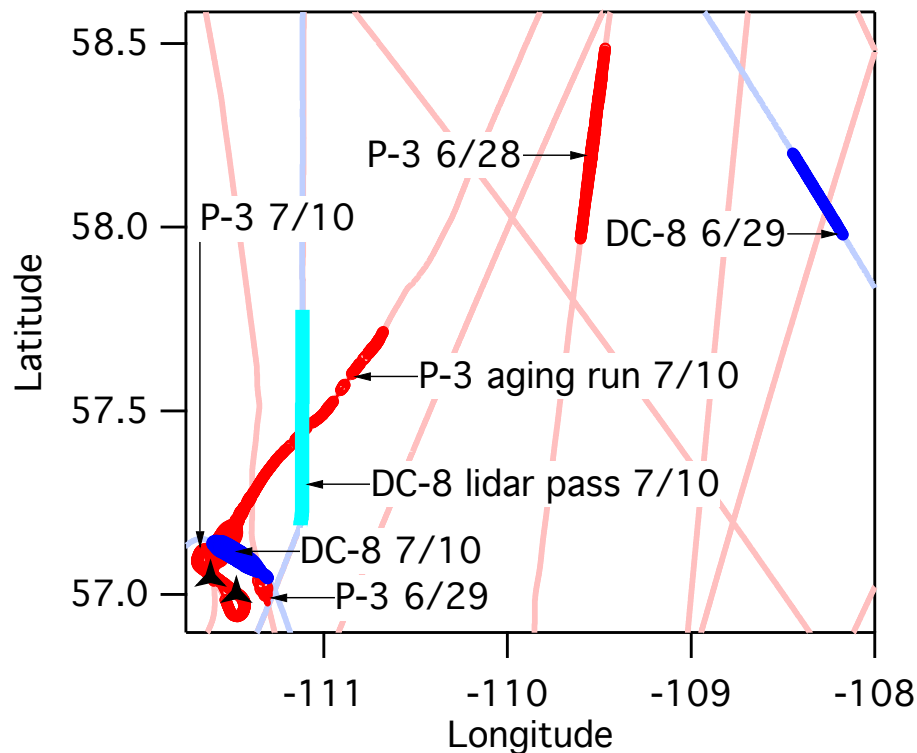


**Fig. 3.** Flight tracks during ARCTAS that passed near the oil sands facilities. Red traces are the P-3B; DC-8 tracks are blue. Emphasized sections are where the aircraft intercepted the plume.

[Title Page](#)[Abstract](#)[Introduction](#)[Conclusions](#)[References](#)[Tables](#)[Figures](#)[◀](#)[▶](#)[◀](#)[▶](#)[Back](#)[Close](#)[Full Screen / Esc](#)[Printer-friendly Version](#)[Interactive Discussion](#)

## Particulate emissions from Athabasca oil sands

S. G. Howell et al.

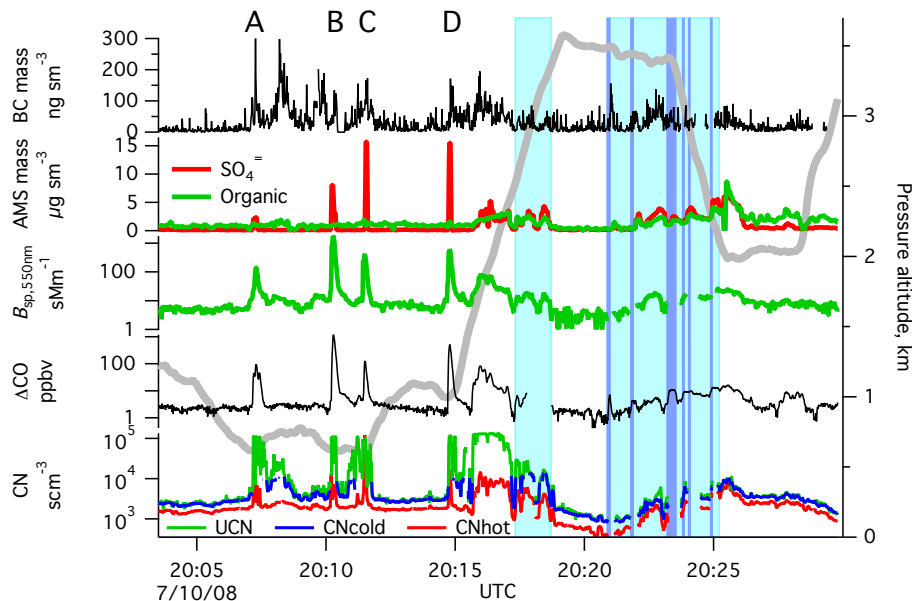


**Fig. 4.** Data along the P-3B flight track shown in Fig. 1. Syncrude upgrader plume penetrations occurred at points A, B, and D, while the Suncor plume was encountered at point C. Light blue regions indicate periods when the plane was among clouds; darker blue shows cloud penetrations. Note that the UCN and CN saturate at  $1 \times 10^5 \text{ cm}^{-3}$  and  $3 \times 10^4 \text{ cm}^{-3}$ , respectively; actual values are higher than shown. The AMS was on a 5 s cycle, blanking half the time, so may have missed peak concentrations. CN, CO, and scattering ( $B_{sp}$ ) are on log scales; CO has the minimum concentration of 93.6 subtracted. The light blue background shows periods among clouds; darker blue indicates cloud penetrations.

Title Page

Abstract

Introduction

Conclusions

References

Tables

Figures

◀

▶

◀

▶

Back

Close

Full Screen / Esc

Printer-friendly Version

Interactive Discussion



## Particulate emissions from Athabasca oil sands

S. G. Howell et al.

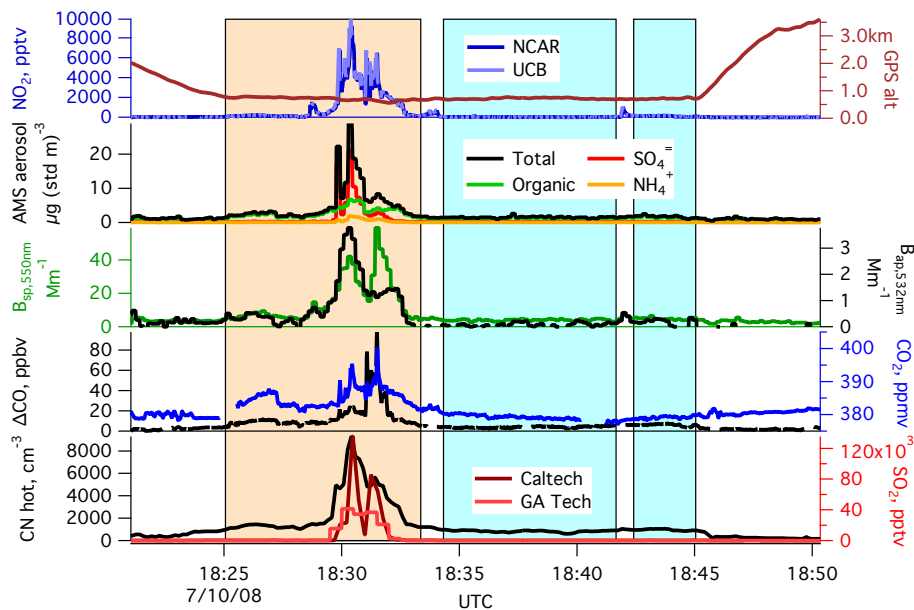


**Fig. 5.** The oil sands plume as seen by in-situ instruments on the DC-8. The light blue region was when the plane was upwind of the facilities, while light brown indicates the plume. The plane flew parallel to the wind at 18:34 UTC, so no flux could be calculated. The gap at 18:43 UTC is there because of the  $\text{NO}_2$  and  $B_{\text{ap}}$  spikes, which appear consistent with diesel truck traffic. The period from 18:25 to 18:28 UTC was downwind of both mining operations and the town of Ft. McMurray.

[Title Page](#)
[Abstract](#)
[Introduction](#)
[Conclusions](#)
[References](#)
[Tables](#)
[Figures](#)
[Back](#)
[Close](#)
[Full Screen / Esc](#)
[Printer-friendly Version](#)
[Interactive Discussion](#)

## Particulate emissions from Athabasca oil sands

S. G. Howell et al.

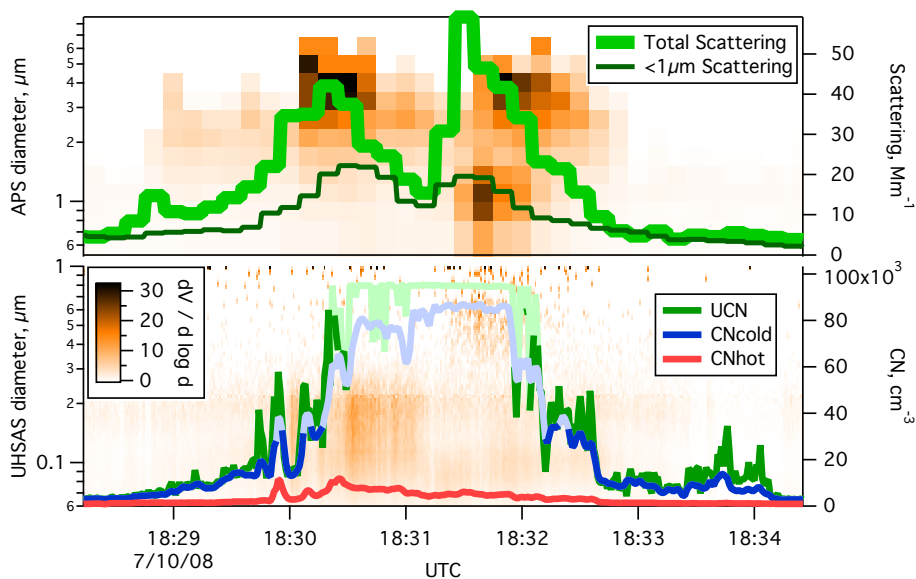


**Fig. 6.** Aerosol volume superimposed on some of the data from Fig. 5. The upper panel shows total and submicron light scattering at 550 nm and the coarse aerosol volume distributions measured by the APS. The lower panel shows UCN, CNcold and CNhot over sub- $\mu\text{m}$  volume distribution from the UHSAS. Pale traces show UCN and CNcold saturation; true values are higher.

Title Page

Abstract

Introduction

Conclusions

References

Tables

Figures

◀

▶

◀

▶

Back

Close

Full Screen / Esc

Printer-friendly Version

Interactive Discussion



## Particulate emissions from Athabasca oil sands

S. G. Howell et al.

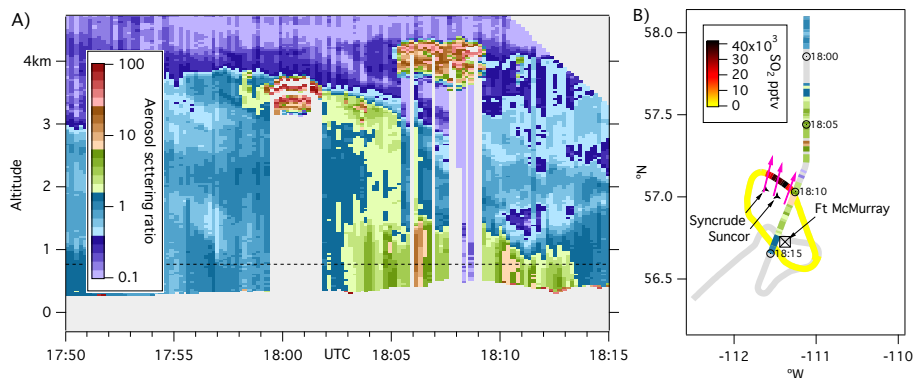


**Fig. 7. (A)** Near infrared (1064 nm) lidar curtain as the DC-8 approached the oil sands area. Gray areas are the blanking interval around the plane, below ground level, or obscured by cloud. The plume is obvious starting at about 18:03 UTC with a maximum at 18:06 UTC. Note that cloud partly obscures the peak, so the aerosol scattering ratio is an underestimate. **(B)** Location of the curtain with respect to sources and the plume as observed in situ. The track from 17:50 to 18:15 UTC is colored with the lidar curtain data from 765 m (dashed line on plot **(A)**), while the low altitude loop is colored by SO<sub>2</sub> concentration. Magenta arrows show 2 h of wind advection as measured by the DC-8.

Title Page

Abstract

Introduction

Conclusions

References

Tables

Figures

◀

▶

◀

▶

Back

Close

Full Screen / Esc

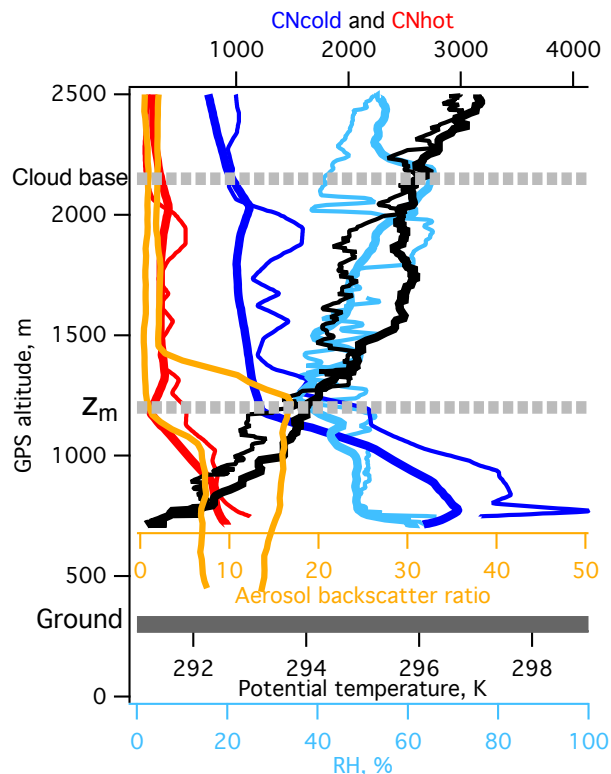
Printer-friendly Version

Interactive Discussion



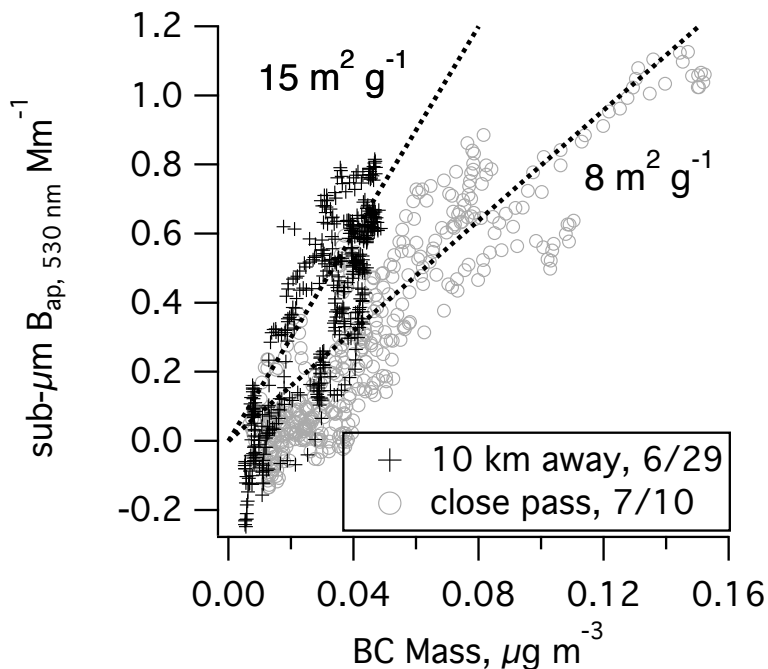
## Particulate emissions from Athabasca oil sands

S. G. Howell et al.



**Fig. 8.** Vertical profile data from the DC-8 near the oil sands plume. Aerosol backscatter ratios are from 18:06:20 UTC (near the peak of the plume downwind of the sampling loop) and 18:10:20 UTC (near where the lidar curtain crossed the sampling loop). Other data are from the descent into and ascent out of the sampling leg, which occurred upwind of the emissions sources. Despite the obvious convection, potential temperature indicates a surprisingly stable boundary layer. In contrast, water vapor and RH suggest that the mixed layer extends to near cloud base at 2.0 to 2.2 km.

[Title Page](#)
[Abstract](#)
[Introduction](#)
[Conclusions](#)
[References](#)
[Tables](#)
[Figures](#)
[◀](#)
[▶](#)
[◀](#)
[▶](#)
[Back](#)
[Close](#)
[Full Screen / Esc](#)
[Printer-friendly Version](#)
[Interactive Discussion](#)

**Fig. 9.** Relationship between BC mass and aerosol light absorption from the P-3 from directly over the upgrader facilities (10 July) and from about 10 km downwind. 1 s data have been smoothed with a 21 point box filter, and periods on 10 July where the PSAP fluctuated wildly due to humidity transitions in the plumes have been eliminated. The dotted lines are not fits to the data; they are shown to illustrate that the data obtained were similar to literature values for uncoated ( $8 \text{ m}^2 \text{ g}^{-1}$ ) and coated ( $15 \text{ m}^2 \text{ g}^{-1}$ ) soot.

**Particulate emissions from Athabasca oil sands**

S. G. Howell et al.

Title Page	
Abstract	Introduction
Conclusions	References
Tables	Figures
◀	▶
◀	▶
Back	Close
Full Screen / Esc	
Printer-friendly Version	
Interactive Discussion	



## Particulate emissions from Athabasca oil sands

S. G. Howell et al.

Title Page

Abstract

Introduction

Conclusions

References

Tables

Figures

◀

▶

◀

▶

Back

Close

Full Screen / Esc

Printer-friendly Version

Interactive Discussion

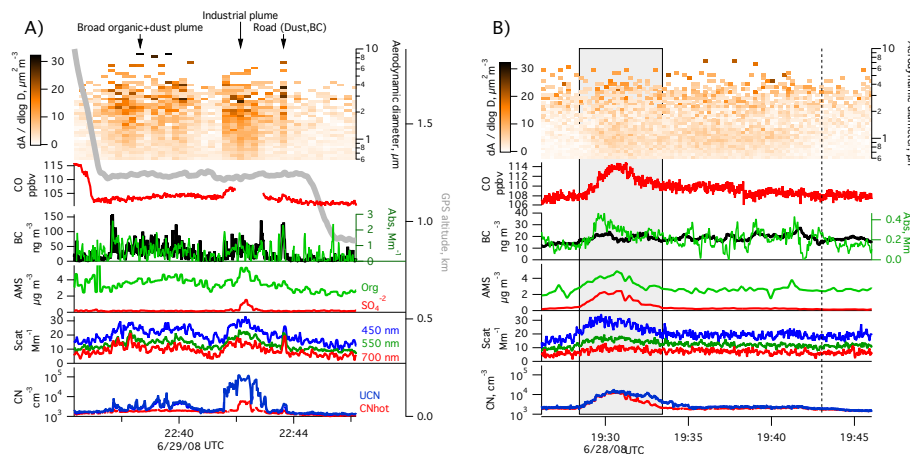


**Fig. 10.** P-3B crossings of the oil sands plume at **(A)** about 10 km (on 29 June) and **(B)** about 180 km (28 June) from the upgraders. Vertical scales are the same on both plots except for CO, BC, and absorption. Absorption is for 530 nm light. The gap in CO data around 22:42 UTC on 29 June was due to an automatic calibration cycle. Altitude on 28 June was constant at 1200 m, so is not shown. Low BC and absorption rendered the data sufficiently noisy that a 21 s box filter was applied to make changes visible. The gray region shows the minimal plume period used to calculate fluxes in Table 1, defined by the enhanced  $\text{SO}_4^-$ . The vertical dashed line marks the end of the maximum plume period, determined from BC and the  $1 \mu\text{m}$  mode visible in the APS data.

**Particulate emissions from Athabasca oil sands**

S. G. Howell et al.

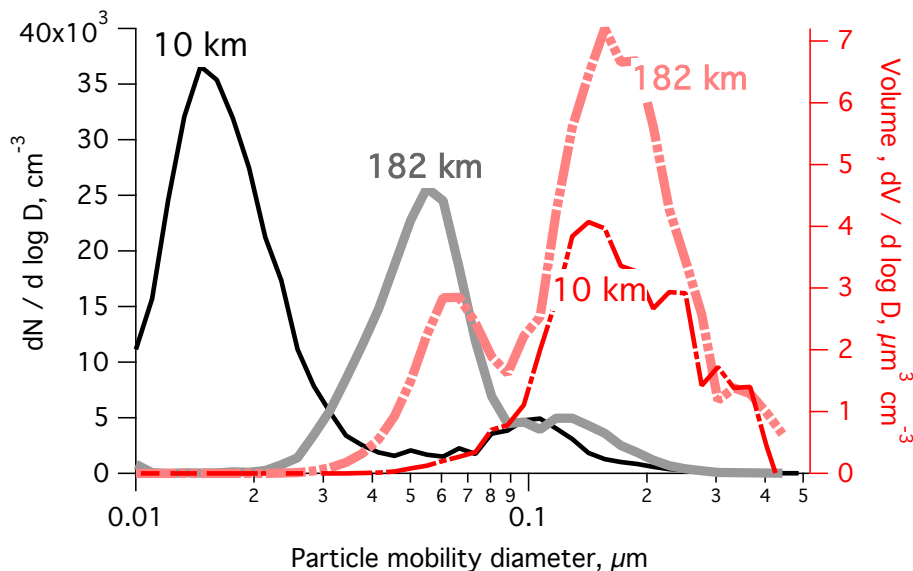


**Fig. 11.** DMA size distributions obtained 10 and 180 km from the source.

Title Page

Abstract Introduction

Conclusions References

Tables Figures

◀ ▶

◀ ▶

Back Close

Full Screen / Esc

Printer-friendly Version

Interactive Discussion



## Particulate emissions from Athabasca oil sands

S. G. Howell et al.

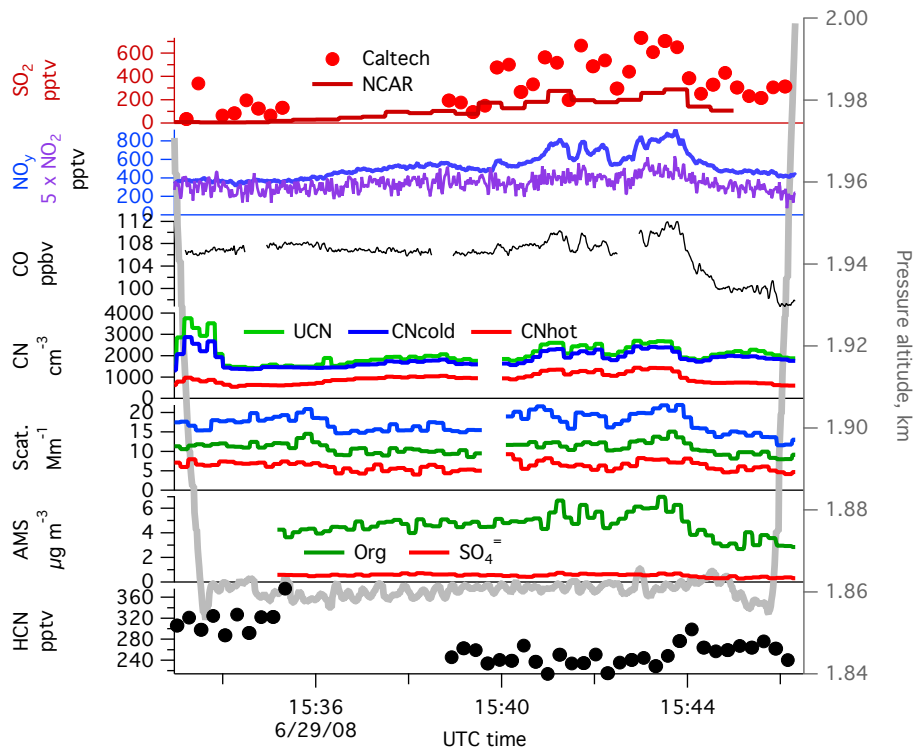


**Fig. 12.** DC-8 plume interception on 29 June.  $\text{NO}_2$ ,  $\text{NO}_y$ , and  $\text{SO}_2$  are consistent with the oil sands plume; low HCN and minimally enriched CO indicate that this is not a fire plume.

Title Page

Abstract

Introduction

Conclusions

References

Tables

Figures

◀

▶

◀

▶

Back

Close

Full Screen / Esc

Printer-friendly Version

Interactive Discussion



## Particulate emissions from Athabasca oil sands

S. G. Howell et al.

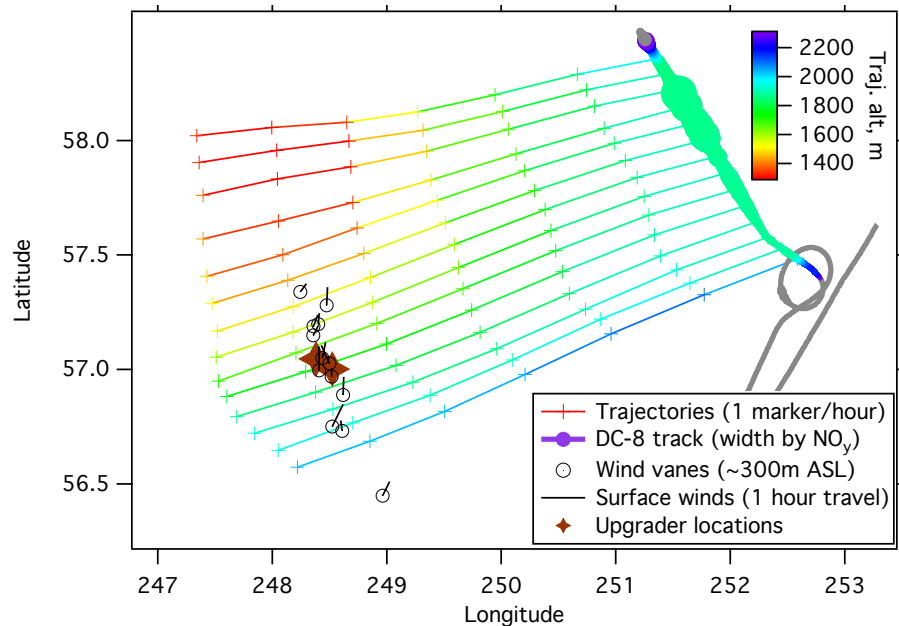


**Fig. 13.** Low altitude winds and back trajectories to the DC-8 flight track on 29 June. Kinematic back trajectories are from the Florida State University group and are driven by hourly FSU/WRF winds on a 45 km grid initialized from GFS. Surface winds are from ground stations at about 5 h before the DC-8 flight.

[Title Page](#)[Abstract](#)[Introduction](#)[Conclusions](#)[References](#)[Tables](#)[Figures](#)[◀](#)[▶](#)[◀](#)[▶](#)[Back](#)[Close](#)[Full Screen / Esc](#)[Printer-friendly Version](#)[Interactive Discussion](#)